Experimental and theoretical characterization of the structure of defects at the pyrite $FeS_2(100)$ surface

K. Andersson,[1,2,3] M. Nyberg,[1] H. Ogasawara,[2] D. Nordlund,[1] T. Kendelewicz,[3] C. S. Doyle,[3] G. E. Brown, Jr.,[2,3] L. G. M. Pettersson,[1] and A. Nilsson[1,2]

[1]*FYSIKUM, Stockholm University, SCFAB, S-10691 Stockholm, Sweden*

[2]*Stanford Synchrotron Radiation Laboratory, 2575 Sand Hill Road, Menlo Park, California 94025, USA*

[3]*Department of Geological and Environmental Sciences, Stanford University, Stanford, California 94305-2115, USA*

(Received 10 June 2004; revised manuscript received 10 August 2004; published 5 November 2004)

Defect-free pyrite (100) surfaces were generated and a controlled manipulation of sulfur defect density at these surfaces was performed. Sulfur species of different coordination environments at the surface were probed by S 2*p* photoemission in combination with theoretical modeling of S 2*p* core-level shifts. A strict structural assignment of S 2*p* peaks at the $FeS_2(100)$ surface in the low defect density regime was achieved. Based on our results, a defect that is related to a surface sulfur vacancy is confirmed to provide the active site for the rapid initial oxidation of pyrite.

DOI: 10.1103/PhysRevB.70.195404 PACS number(s): 73.20.−r, 82.65.+r, 82.80.Pv, 91.60.Ed

I. INTRODUCTION

Pyrite (FeS_2) is the most abundant and widespread sulfide mineral in the Earth's crust and is rich in concentration around deep-sea high-temperature hydrothermal vents (black smokers)[1] and can be found in many rock types including, e.g., coal and lignite beds, sedimentary rocks (including some limestones) and in soils when reducing conditions pertain.[2] The properties of pyrite surfaces have been thought to facilitate the origin of life in the iron-sulfur world scenario[3] and are important to numerous geochemical, industrial and environmental processes including the rapid alteration of pyrite in oxidizing environments generating acid mine drainage (AMD) water from base-metal and precious-metal sulfide mines.[4] Pyrite has indistinct (100) cleavage and fractures conchoidally to unevenly. The (100) surface is also the predominant growth surface of natural pyrite crystals.[5] Pristine $FeS_2(100)$ fracture surfaces are characterized by highly reactive species that are believed to be related to defects caused by sulfur deficiencies.[5–7] Knowledge of the structural properties of possible defects at the pyrite surface is of fundamental importance for understanding their electronic structure and reactivity, including the initiation of oxidation reactions leading to AMD.

Pyrite crystallizes in the cubic NaCl-structure with Fe^{2+} in the Na^+ sites and dimer sulfur anions S_2^{2-} with center of mass located at the Cl^- sites with their molecular axes aligned along the four equivalent $\langle 111 \rangle$ directions. Previous experimental[8–13] and theoretical studies[13–16] of $FeS_2(100)$ have found that the surface can be essentially regarded as a truncation of the bulk structure along a plane of broken Fe–S bonds with no major geometric relaxation.

Core level binding energies are highly sensitive to the local environment of an atom and differing local environments result in core level shifts (CLS). S 2*p* photoemission studies of the pyrite $FeS_2(100)$ surface have mostly been carried out on surfaces produced by fracturing. Various interpretations of the S 2*p* photoemission have been suggested from studies employing photon energies yielding surface-sensitive S 2*p* spectra.[5,8,17,18] The S 2*p* photoemission has been analyzed in terms of one bulk and two surface related contributions, and this picture is now well established for these clean fracture surfaces.[5,7,8,17,19] A third surface-related contribution was recently resolved.[19] However, the interpretation of the S 2*p* photoemission has been based on chemical intuition,[5] and so far no theoretical modeling of either surface sulfur defects or spectroscopic data has been performed to gain structural insights at the atomic level.

In the present letter we report on the generation of defect-free pyrite $FeS_2(100)$ surfaces and a controlled manipulation of defect density at these surfaces. The S 2*p* photoemission was studied, and, in combination with spectroscopic modeling using density functional theory (DFT), this provides a strict structural interpretation of the S 2*p* photoemission. The structural defect that is the active site for rapid initial oxidation at the pyrite (100) surface is assigned to a sulfur monomer with bulk-like local Fe-coordination.

II. DETAILS OF EXPERIMENT AND CALCULATIONS

A. Experiment

Experiments were performed at the surface science branch-line of the undulator beamline I511 at the Swedish national synchrotron radiation facility MAXLab in Lund, Sweden.[20] Sulfur 2*p* photoemission spectra were recorded at room temperature under ultra high vacuum (UHV) conditions. The S 2*p* spectra were taken with total energy resolution of 100, 120, 190, and 240 meV for excitation energies of 225, 415, 755, and 960 eV, respectively. The pyrite sample used was a 1 cm^2 and 2 mm thick slice cut from a natural (100) single crystal from Navajun, Spain. A 200 V Ne^+-sputtering procedure was used to obtain a clean surface under UHV conditions. The ion-sputtering preferentially removes lighter elements and therefore removes S to a higher degree than Fe. Since annealing causes additional removal of S, defect-free surfaces could not be obtained by a simple annealing procedure of the sputtered sample. However,

defect-free surfaces were obtained by annealing the sample in 1×10^{-7} Torr S_2(g) at 570 K for 10 min. In addition, surfaces with controlled defect densities were generated through mild Ne^+-sputtering of defect-free surfaces prepared by the method described above.

B. Calculations

All calculations were performed within the DFT framework as implemented in the DACAPO code.[21] Electron–ion interactions were included through the use of ultrasoft pseudopotentials[22] within a plane wave basis with a cutoff energy of 340 eV. Electron exchange and correlation effects were described by the Perdew Wang (PW91) generalized gradient approximation.[23] The FeS_2(100) surface was modeled by a periodic array of four to five FeS_2 layers (12 to 15 atomic layers) and a sufficient vacuum separation (>10 Å) with dipole corrections for further efficient decoupling of the slabs. Geometry optimization of the defect-free surface was performed with a $p(1\times1)$ surface unit cell and a Monkhorst-Pack[24] mesh with $4\times4\times1$ k-point sampling within the surface Brillouin zone. A larger $p(2\times1)$ surface unit cell was employed for geometry optimization of structural defects and core hole calculations. Similar mesh points as for the $p(1\times1)$ surface unit cell were used. The $p(2\times1)$ cells were arranged in a laterally overlapping brick wall structure resulting in a square symmetry of defects and simulated core holes in the slab. Interaction between core holes in repeat units of the $p(2\times1)$ cell was negligible as evidenced by comparison with calculated core level shifts for an extended $p(2\times2)$ cell.

The Z+1 approximation, also known as the equivalent core approximation, has successfully been applied for CLS in metallic systems.[25] At the heart of the Z+1 theoretical approach for CLS lies the basic assumption of an electronically completely screened final state, i.e., a state in which the conduction electrons have attained a fully relaxed configuration in the presence of a core hole. Final state effects are essential for understanding CLS in metallic systems and this has been found to hold true in semiconducting systems as well.[26] Pyrite is a semiconductor, and the S 2*p* CLS can be calculated within the Z+1 approximation by comparing total energies of core ionized (Z+1) final state systems for which the unperturbed initial state systems are identical.[27] By replacing the sulfur pseudopotential with one for chlorine at the selected site in the slab we can thus obtain the relative CLS between modeled core hole sites as the total energy difference.

III. RESULTS AND DISCUSSION

The S 2*p* photoemission spectrum from a defect-free sample is shown in Fig. 1(a). The spectra simply consist of two separable types of S 2*p* features, one $2p_{3/2}$ component at 161.75 eV, labeled S, and the other at 162.35 eV, labeled B, with their respective spin-orbit split $2p_{1/2}$ component at 1.19 eV higher binding energy.[28] From a peak fitting procedure, we found a minor feature at about 161.25 eV that could not be fit using lineshapes and binding energies of other S 2*p*

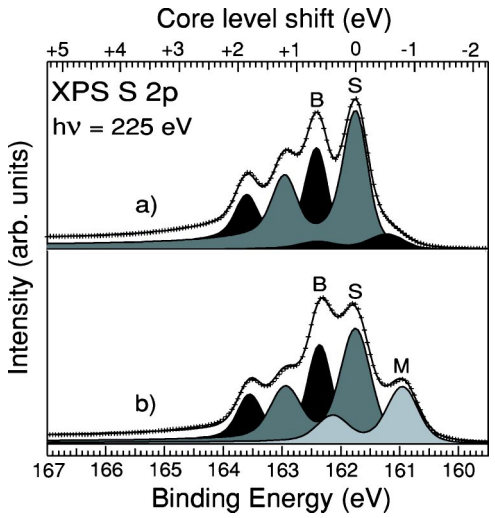

FIG. 1. S 2*p* XPS at an excitation energy of 225 eV for defect-free and low defect density pyrite (100). Spectra are normalized to the same area. Experimental spectra are shown as crosses; solid lines are the results from peak fitting. (a) Defect-free and (b) low defect density surface after 10 min of 200 V Ne^+-sputtering. A new S $2p_{3/2}$ feature, labeled M, is generated at a binding energy of 160.95 eV.

components found in this study. The feature was fit with a S $2p_{3/2}$ component at 161.25 eV and an intensity of 10%–15% of the S-component. We believe this component to be related to specific sulfur species located at step edges. The 161.25 eV feature has not been resolved at pyrite (100) surfaces prepared by fracturing. It is therefore expected to have only a very small impact on the reactivity of fractured pyrite surfaces if present at fracture-surfaces at all. This feature will not be further discussed in the present paper.

We now introduce a small amount of defects into the system by bombarding the surface with Ne^+-ions for 10 min and the result of this procedure can be seen in Fig. 1(b). We observe that a new $2p_{3/2}$ feature, labeled M, appears at a binding energy of 160.95 eV mostly at the expense of spectral intensity of the species related to the S-component but also with a small contribution from the spectral intensity related to the B-species. This M-species has been shown to be by far the most reactive species at the onset of pyrite oxidation in air on (100) surfaces prepared by fracturing.[7] The spectrum of the low defect density surface in Fig. 1(b) is essentially identical with those from vacuum-fractured surfaces.[5,7,8,17–19] More prolonged sputtering results in a S 2*p* photoemission spectrum with the defect-related M feature intensity increased mostly at the expense of the S-component. In addition, a very weak new component is observed around 0.8 eV below M, i.e., −1.6 eV relative to the S-component. This feature agrees very well with the component around 0.6 eV below M, i.e., −1.4 eV relative to the S-component, found in the study by Leiro *et al.*[19]

The escape depth of photoelectrons with kinetic energies greater than ~50 eV increases with kinetic energy.[29] By varying the incident photon energy, we are able to change kinetic energies and thereby the effective probing depth as indicated by the photon energy dependence of the S 2*p* pho-

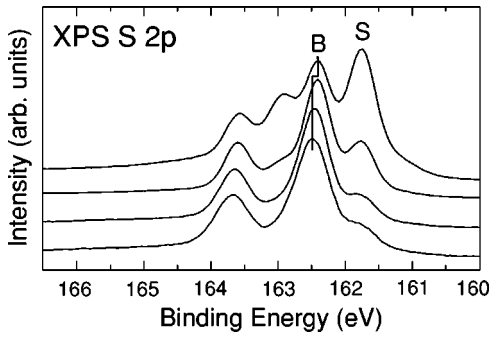

FIG. 2. Photon energy dependence of the S 2*p* photoemission of the defect-free pyrite (100) surface as in Fig. 1(a) at, from top to bottom, 225, 415, 755, and 960 eV photon energy, respectively. All spectra were normalized to the same background; the constant background was then subtracted and the B-component was normalized to the same height for all spectra. The S-component is clearly surface-related as seen from the photon energy dependence. The +0.1 eV shift of the B-component with increasing photon energy is indicated by the solid line.

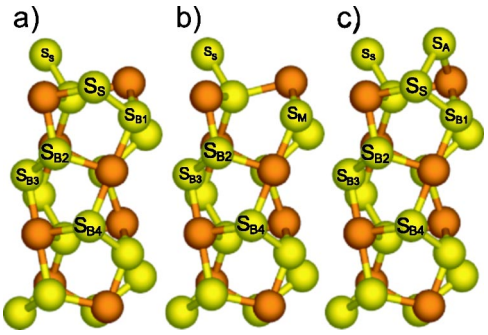

FIG. 3. (Color online). Side-views of different species and structural situations at the $FeS_2(100)$ surface used for the spectroscopic modeling shown together with their labeling. (a) Defect-free bulk terminated surface. (b) Surface sulfur vacancy, resulting in the sulfur monomer species S_M. (c) Situation generated at opposite cleavage face from the surface sulfur vacancy resulting in the S_A-species.

toemission from the defect-free sample [Fig. 1(a)] shown in Fig. 2. It is clear from the data that the S- and B-features are surface and bulk related, respectively. We also found that the CLS between the two components S and B increases gradually from +0.61 to +0.71 eV for the highest used excitation energy of 960 eV. This may indicate that feature B at highest surface sensitivities contains some contribution from an unresolved subsurface component(s) at lower binding energy. The same photon energy dependence investigation of the S 2*p* photoemission was undertaken for the low defect density sample in Fig. 1(b) (not shown). Based on the results, which were in good agreement with other photon energy dependent studies of the S 2*p* photoemission on the vacuum-fractured surface,[19] we conclude the M-component to be surface related. From the photon energy dependent study of the low defect density surface we furthermore find the B-component to shift by +0.1 eV relative to both the S- and M-component for photon energies between 225 and 960 eV. The observed shift of the subsurface and bulk-like B-component with kinetic energy is consistent with a conventional XPS study (1487 eV photon energy) where a CLS between the S- and B-component as large as +0.8 eV was reported.[30]

To understand the origin of the components in the S 2*p* photoemission we turn to theoretical modeling and consider three types of structural scenarios for sulfur at the (100) fracture surface as plausible candidates. The first is the result from a surface generated by Fe–S bond breaking only; see Fig. 3(a). This represents the defect-free bulk-terminated $FeS_2(100)$ surface. Figure 3(b) shows the second scenario where one S_S is missing due to a S_S–S_{B1} bond breakage, resulting in a bulk-like Fe-coordinated sulfur monomer, S_M, at the surface. The third and final scenario, as shown in Fig. 3(c), includes the counter-species, S_A, which would form at the opposite cleavage surface due to a S_S–S_{B1} bond breakage. The sulfur species, their labeling, and their respective geometries for which the CLS were calculated are shown in Fig. 3.

The relaxation of the defect-free bulk terminated surface shown in Fig. 3(a) was performed with the DACAPO code and followed very closely previous theoretical work.[15,16] As was also found in previous studies,[15,16] surface relaxation is characterized by a 0.1 Å contraction of the topmost first surface-Fe layer towards the bulk, leading to a shortening of the surface-Fe–S_{B2} bond by 0.1 Å. Furthermore, a 0.08 Å elongation of the S_{B1}–second-layer-Fe bond was noticed. For the scenarios in Figs. 3(b) and 3(c), the geometrical changes were negligible except around the specific defect. The most significant structural change for the case of the surface sulfur vacancy in Fig. 3(b) was a +0.15 Å difference in position of S_M along the surface normal compared to S_{B1} in Fig. 3(a). This is caused mainly by an elongation of the second layer Fe–S_M bond by 0.08 and a +0.04 Å displacement of the second layer Fe, which binds to S_M, along the surface normal compared to the situation in Fig. 3(a). The S_A-species in Fig. 3(c) was found to coordinate to S_S resulting in a S_A–S_S bond length of 2.26 Å and a surface-Fe–S_A bond length of 2.29 Å.

The results of the calculated CLS relative to S_S for the different sulfur species considered are summarized and compared to our experimentally observed CLS in Table I. We find from our modeling results that a core hole created on S_{B1}, as in the situation of the defect-free (bulk-terminated) surface [see Fig. 3(a)], is shifted +0.53 eV relative to a core hole generated on S_S. We therefore assign the features at 161.75 and 162.35 eV to core holes generated at S_S and S_{B1}, respectively.

We find variations of the calculated CLS of bulk-like coordinated S-atoms near the defect-free surface in Fig. 3(a). This CLS variation (from the surface downward: +0.53, +0.75, +0.58, +0.72 eV) is most likely induced by surface relaxation. The variation of calculated CLS near the surface could explain the apparent +0.1 eV gradual shift of the B-component with increased photon energy, i.e., probing depth. The calculated CLS in the third layer of a five-layer slab (S_{B4}) was found to be +0.72 eV compared to +0.53 for S_{B1}. Structural relaxation effects were negligible in the third layer, and S 2*p* binding energies for sulfur dimers deeper in the bulk are thus expected to be very similar to those in the third layer.

The structural models in Figs. 3(b) and 3(c) result from breakage of a S–S bond. The surface-related feature M in

TABLE I. Comparison of experimental CLS in the S 2*p* photoemission spectra from Figs. 1 and 2. with calculated CLS for different structural situations of sulfur as depicted in Fig. 3. The CLS were calculated relative to the total energy of a simulated core hole in the Z+1 approximation at S_S at the defect-free bulk terminated situation for the specific supercell used. In the defect-configurations, Figs. 3(b) and 3(c), this was achieved by modeling the S_S core-hole at the opposite defect-free surface of the slab.

	S/S_S	B	S_{B1}	S_{B2}	S_{B3}	S_{B4}	M/S_M	S_A
Experimental CLS (eV)	0	+0.61−0.71					−0.80	−1.4 (Ref. 19)
Theoretical CLS (eV)	0		+0.53	+0.75	+0.58	+0.72	−0.98	−1.37

the S 2*p* XPS spectra of pyrites has previously been assigned to sulfur monomers.[5,8,18,19] We find in Table I that a core hole created at the sulfur monomer S_M [Fig. 3(b)] is shifted by −0.98 eV as compared to S_S in the surface dimer. The rather good agreement with the experimental −0.80 eV CLS makes it plausible to assign the M-peak at 160.95 eV to a sulfur monomer created as the result of the loss of S_S in the surface dimer. This assignment is furthermore consistent with the generation of surface sulfur vacancies by Ne^+-sputtering. The recently resolved low-intensity surface-related feature from a pyrite (100) surface prepared by fracturing in vacuum[19] at about 160.35 eV (−1.4 eV CLS relative to the S-component) is found to correspond very well with the configuration depicted in Fig. 3(c) with a core hole at the sulfur ad-atom S_A created as a counter-species to the sulfur vacancy at the surface.

IV. CONCLUSIONS

In conclusion, we have generated defect-free pyrite FeS_2(100) surfaces under UHV conditions and have devised a method to control sulfur defect density at the surface. Variation in surface defect density among pyrite samples prepared using different protocols in different studies is a reason for differences in observed reactivities of pyrite (100) surfaces reported in the literature. Our ability to generate defect-free surfaces and to control the defect density, in combination with our calculations, unambiguously relates sulfur defects to S−S bond breaking and provides a basis for interpretation of the high reactivity of species related to the S $2p_{3/2}$ XPS spectral component at 160.95 eV. The most prominent surface sulfur defect generated on the fractured surface was assigned to a point-defect-like sulfur vacancy. The removal of a topmost S atom leaves behind a sulfur monomer without changing local Fe-coordination at the surface. The structural identification of S-species from the S 2*p* photoemission study was achieved by total energy calculations along with use of the conceptually simple Z+1-approximation.

ACKNOWLEDGMENTS

This work was supported by NSF Grant No. CHE-0089215, the Swedish Foundation for Strategic Research, the Swedish Natural Science Research Council, and the U.S. Department of Energy, Office of Basic Energy Sciences through the Stanford Synchrotron Radiation Laboratory. Generous grants of computer time at the Center for Parallel Computing, Sweden, are gratefully acknowledged. We are indebted to the staff at MAX-lab for valuable assistance.

[1] M. D. Hannington, I. R. Jonasson, P. M. Herzig, and S. Petersen, in *Seafloor Hydrothermal Systems*, edited by S. E. Humphris, R. A. Zierenberg, L. S. Mullineaux, and R. E. Thomson (American Geophysical Union, Washington, DC, 1995); M. K. Tivey, *ibid.*

[2] *Minerals in Soil Environments*, 2nd ed., edited by J. B. Dixon and S. B. Weed (Soil Science Society of America, Madison, WI, 1989); C. Klein, *Manual of Mineral Science*, 22nd ed. (Wiley, New York, 2002).

[3] G. Wächtershäuser, Microbiol. Rev. **52**, 452 (1988); Proc. Natl. Acad. Sci. U.S.A. **87**, 200 (1990); Prog. Biophys. Mol. Biol. **58**, 85 (1992).

[4] V. P. Evangelou and Y. L. Zhang, Crit. Rev. Environ. Sci. Technol. **25**, 141 (1995); D. K. Nordstrom and C. N. Alpers, Proc. Natl. Acad. Sci. U.S.A. **96**, 3455 (1999).

[5] H. W. Nesbitt, G. M. Bancroft, A. R. Pratt, and M. J. Scaini, Am. Mineral. **83**, 1067 (1998).

[6] J. M. Guevremont, J. Bebie, A. R. Elsetinow, D. R. Strongin, and M. A. A. Schoonen, Environ. Sci. Technol. **32**, 3743 (1998).

[7] A. G. Schaufuß, H. W. Nesbitt, I. Kartio, K. Laajalehto, G. M. Bancroft, and R. Szargan, Surf. Sci. **411**, 321 (1998).

[8] C. Pettenkofer, W. Jaegermann, and M. Bronold, Ber. Bunsenges. Phys. Chem. **95**, 560 (1991).

[9] D. Siebert and W. Stocker, Phys. Status Solidi A **134**, K17 (1992).

[10] C. M. Eggleston and M. F. Hochella, Jr., Am. Mineral. **77**, 221 (1992).

[11] C. M. Eggleston, J. Ehrhardt, and W. Stumm, Am. Mineral. **81**, 1036 (1996).

[12] S. Chaturvedi, R. Katz, J. Guevremont, M. A. A. Schoonen, and D. R. Strongin, Am. Mineral. **81**, 261 (1996).

[13] K. M. Rosso, U. Becker, and M. F. Hochella, Am. Mineral. **84**, 1535 (1999).

[14] N. H. de Leeuw, S. C. Parker, H. M. Sithole, and P. E. Ngoepe, J. Phys. Chem. B **104**, 7969 (2000).

[15] A. Hung, J. Muscat, I. Yarovsky, and S. P. Russo, Surf. Sci. **513**, 511 (2002).

[16] A. Stirling, M. Bernasconi, and M. Parrinello, J. Chem. Phys. **118**, 8917 (2003).
[17] M. Bronold, Y. Tomm, and W. Jaegermann, Surf. Sci. Lett. **314**, L931 (1994).
[18] S. Mattila, J. A. Leiro, and K. Laajalehto, Appl. Surf. Sci. **212-213**, 97 (2003).
[19] J. A. Leiro, S. S. Mattila, and K. Laajalehto, Surf. Sci. **547**, 157 (2003).
[20] R. Denecke, P. Väterlein, M. Bässler, N. Wassdahl, S. Butorin, A. Nilsson, J. E. Rubensson, J. Nordgren, N. Mårtensson, and R. Nyholm, J. Electron Spectrosc. Relat. Phenom. **101-103**, 971 (1999).
[21] DACAPO is a free software developed at the Center for Atomic-Scale Materials Physics (CAMP), http://www.fysik.dtu.dk/campos, funded by the Danish Research Council; B. Hammer, L. B. Hansen, and J. K. Nørskov, Phys. Rev. B **59**, 7413 (1999).
[22] D. Vanderbilt, Phys. Rev. B **41**, 7892 (1990).
[23] J. P. Perdew and Y. Wang, Phys. Rev. B **45**, 13244 (1992).
[24] J. D. Pack and H. J. Monkhorst, Phys. Rev. B **16**, 1748 (1977).
[25] B. Johansson and N. Mårtensson, Phys. Rev. B **21**, 4427 (1980); M. Aldén, H. L. Skriver, and B. Johansson, Phys. Rev. Lett. **71**, 2449 (1993).
[26] E. Pehlke and M. Scheffler, Phys. Rev. Lett. **71**, 2338 (1993).
[27] N. Mårtensson and A. Nilsson, J. Electron Spectrosc. Relat. Phenom. **75**, 209 (1995).
[28] The binding energy scale for the S 2*p* spectra is calibrated using the Fermi level of metallic pyrrhotite ($Fe_{1-x}S_x$) and heavily sulfur reduced pyrite. The binding energy of the 160.95 eV species (M-component) at the excitation energy of 225 eV is found to stay constant within 0.05 eV in the low and high defect density regime as well as for thermally decomposed pyrite (pyrrhotite, $Fe_{1-x}S_x$) in our experiments.
[29] D. R. Penn, Phys. Rev. B **13**, 5248 (1976).
[30] S. Karthe, R. Szargan, and E. Suoninen, Appl. Surf. Sci. **72**, 157 (1993).